Int. J. Electrochem. Sci., 15 **(2020)** 4811 – 4826, doi: 10.20964/2020.05.43

International Journal of
ELECTROCHEMICAL
SCIENCE
www.electrochemsci.org

Large-scale preparation of fluorographene/epoxy nanocomposite coatings on steel for corrosion protection

Meng Yang[1], *DanDan Li*[1], *Haoyang Sun*[1], *Fan Lei*[1,2,*], *Yi Huang*[2], *Dazhi Sun*[1,*]

[1] Department of Materials Science and Engineering, Southern University of Science and Technology, Shenzhen, Guangdong 518055, China
[2] School of Materials Science and Engineering, Nankai University, Tianjin, 300071, China
[*]E-mail: leif@sustech.edu.cn (Fan Lei), sundz@sustech.edu.cn (Dazhi Sun)

Received: 17 December 2019 / *Accepted:* 8 March 2020 / *Published:* 10 April 2020

Graphene, due to its unique two-dimensional structure and superior barrier property, is considered as an excellent filler in organic coatings used for the corrosion protection of metals. However, it has also been found to promote the metal corrosion because of its high electrical conductivity. In this work, we used electrically insulated fluorographene (FG) nanoplatelets as fillers for epoxy coatings and investigated their corrosion protection properties for metals. FG was prepared by a microwave-assisted liquid phase exfoliation method and then was incorporated into epoxy matrix through an environment-friendly solventless method. The electrochemical impedance spectroscopy (EIS) and the potentiodynamic polarization measurements show that the prepared FG/epoxy nanocomposite coatings exhibit superior anticorrosion performance, which are improved by one order of magnitude compared with the pure epoxy coating. The improvement of the corrosion resistance of the nanocomposite coatings is mainly attributed to the barrier properties and electrical insulation of FG nanoplatelets. Moreover, the nanocomposite coating containing 0.5 wt% FG shows the best anticorrosion performance because of the uniform dispersion of a small amount of FG nanoplatelets in the epoxy matrix.

Keywords: metal protection, epoxy coating, fluorographene, corrosion resistance

1. INTRODUCTION

As one of the most important structural materials, metal has a close relationship with our life and has been applied in lots of industrial fields, i.e., automotive machine, construction and household appliances due to its outstanding properties [1]. However, the corrosion of metal is still a severe problem for its applications, which may cause potential safety problems and high economic costs, especially in some harsh environments [2, 3]. Hence, extensive studies on metal corrosion protection have been carried out [4-8]. Organic coating protection is used as a facile, economic and effective method to delay the process of metal corrosion [9, 10]. In this regard, organic coating can provide protection for metal

structure mainly through physically isolating the metal substrate from the corrosive environment [11]. Unfortunately, organic coatings suffer from some problems during use. It is reported that corrosive mediums such as oxygen, water and chloride ion can easily permeate coatings and reach the interface between metal and coating, leading to the decline of coating adhesion and the promotion of metal corrosion beneath coatings [12]. Therefore, pure organic coatings could hardly provide a long-term corrosion protection for metal [1, 13, 14].

In order to enhance the anticorrosion performance of organic coatings, i.e., widely used epoxy coatings, different methods have been attempted extensively [5, 10, 15-19]. Incorporating various fillers into epoxy was applied as the most effective method to enhance the anticorrosion performance of epoxy coatings by preventing the diffusion of corrosive mediums [12]. Compared to micron size fillers, e.g. zinc phosphates [20, 21], lamellar aluminum pigment [22] and ferrite inhibition pigment [23], nano-fillers can provide better corrosion protection properties for epoxy matrixes due to their smaller particle sizes and higher specific surface areas [11]. In the last few years, various composite coatings have been studied and reported, which use different nano-fillers, including silicon dioxide [24], titanium dioxide [25], zinc oxide [26] and clay [27], and the results show that the barrier properties of the coatings were enhanced significantly through incorporating nano-fillers into epoxy even with few fillers. Recently, graphene and its derivatives have been in the center of attention as nano-fillers for polymeric coatings to extend their corrosion protection properties [28-30].

Graphene, a representative two-dimensional layered material, has many outstanding properties which are ideal for corrosion protection applications, including molecular impermeability, excellent chemical and thermal stability and high light transparency [31-35]. Chang et al. [4] successfully prepared polyaniline/graphene composites coating for metal corrosion protection. They demonstrated that the composite coatings showed excellent impermeability to O_2 and H_2O, thus providing good corrosion protection for steel. However, graphene also shows some disadvantages for the corrosion protection applications. Cui et al. [36] stated that graphene can accelerate localized corrosion due to galvanic reaction at exposed graphene-metal interfaces. Sun et al. [37] introduced graphene into polyvinyl butyral coating for the corrosion protection of copper. The scratch test demonstrated that the graphene/ polyvinyl butyral composite coatings can cause the corrosion promotion of the copper substrates because of the intrinsic electrochemical properties of graphene when coatings were damaged. Besides, graphene easily aggregates together when applied in coatings on account of strong van der Waals forces between graphene nanosheets, which strongly distort the barrier properties of the material. Therefore, covalent or non-covalent functionalization need to be used to improve the dispersion of graphene in polymeric coatings which is complicated and may lead to environmental pollution [15, 38, 39]. Fluorographene (FG), as a derivative of graphene, not only inherits the superior chemical and thermal stability of graphene, but also shows unique electrical insulation property which is desired for corrosion protective materials [40-42]. Moreover, it has been demonstrated that FG nanoplatelets show good dispersion in the amine curing agent because hydrogen bonding forms between F atoms and $-NH_2$ [43]. Therefore, it is supposed that FG nanoplatelets introduced in epoxy could be dispersed uniformly through using polyetheramine D230 curing agent as an efficient dispersant, thereby further enhancing the corrosion protection properties of the coatings.

In this work, we first prepared FG from graphite fluoride (GrF) by a microwave-assisted liquid phase exfoliation method and then incorporated FG nanoplatelets into epoxy matrix by utilizing D230 curing agent as dispersant without other solvents and surfactants, which is environment friendly. The FG/epoxy nanocomposites with different loadings of FG were used to fabricate corrosion protective coatings for steel. The anticorrosion performance of the FG/epoxy nanocomposite coatings were investigated through long-term immersion tests in 3.5 wt% NaCl aqueous solutions. The effect of FG concentrations on the anticorrosion performance of the epoxy coatings was discussed by means of the cross-section morphology analysis and electrochemical corrosion measurements.

2. EXPERIMENTAL SECTION

2.1. Materials.

GrF powders, used to prepare FG, were bought from Shenyang Xifu technology Co., Ltd. Epoxy 44 resin (E44) was purchased from Shenzhen Jitian Chemical Corporation. Jeffamine D230 hardener and N, N-dimethyl formamide (DMF) was purchased from Aladdin Chemical Corporation. All other solvents and reagents were bought from Aladdin Chemical Corporation and used as received.

2.2. Preparation of FG.

FG was prepared from GrF through a microwave-assisted liquid phase exfoliation method [44]. In a typical experiment, 125 mg GrF powder was added into 25 ml DMF to prepare GrF/DMF suspension, followed by a continuous ultrasonication for 25 min in a sonication bath (Kunshan KQ-300VDE). Subsequently, the suspension was centrifuged for 20 min at 10,000 rpm in a high-speed centrifuge (Cence TG16-WS). The excessive DMF was removed and the precipitate was transferred into a glass culture dish. Then, the culture dish was placed in a microwave oven for 5 min with a power of 800 W for exfoliation. Finally, the exfoliated FG powders in the glass culture dish were collected for further characterizations.

2.3. Preparation of the FG/epoxy Corrosion Protective Coatings.

To prepare the FG/epoxy nanocomposites, 0.1 g FG powder was dispersed in 5 g D230 curing agent by ultrasonicating for 30 min. Successively, 15 g E44 was mixed with the dispersion and the mixture was degassed at 70 °C for 10 min by using a rotary evaporator (IKA RV10) to obtain a homogeneous FG/epoxy nanocomposites. Meanwhile, the Q235 steel substrate surfaces were polished with 240, 800 and 1200 grit papers, then ultrasonically cleaned in acetone for 15 min and dried. Infrared heating tape casting coater (Kejing MSK-AFA-L800) was employed to prepare the FG/epoxy nanocomposite coatings on the steel substrates. Then, the steel substrates coated with nanocomposites were dried at room temperature for 6 h and 70 °C for 12 h, marked as FG-0.5 wt%. Analogously, the organic coatings incorporating different FG contents (0, 0.2, 0.4 and 0.6 g) were also prepared and

marked as FG-0 wt%, FG-1 wt%, FG-2 wt% and FG-3 wt%, respectively. The thickness of all the coatings was controlled to be around 70 μm. The schematic illustration shown in Figure 1 displays the specific preparation processes for the FG/epoxy nanocomposite coatings.

2.4. Characterization

The morphology of GrF was determined by scanning electronic microscope (SEM, Tescan VEGA 3 LMH) and the chemical component was investigated by energy dispersive analysis (EDS, Oxford instrument Aztec X-Max80). Transmission electron microscope (TEM, Tecnai F30) was implemented to observe the morphology of FG nanoplatelets. Atomic force microscopy (AFM, Bruker Dimension) was carried out to quantitatively investigate the thickness of FG nanoplatelets. The cross sections of the FG/epoxy nanocomposite coatings were determined by SEM. The cross-section samples used were obtained by fracturing the coatings in liquid nitrogen with pre-crack. The crystal phase of FG nanoplatelets and the prepared coatings were studied by X-ray diffraction (XRD, Rigaku Smartlab).

Electrochemical impedance spectroscopy (EIS) was use to study the electrochemical properties of the FG/epoxy nanocomposite coatings on CS Electrochemical Workstation (CorrTest CS310H). A conventional three electrode cell [45], consisted of a platinum sheet as counter electrode, an Ag/AgCl/saturated KCl electrode as reference electrode and the coated steel specimen as working electrode was applied for the electrochemical measurement. The EIS measurements were performed at room temperature in 3.5 wt% NaCl aqueous solution in the frequency of 10^{-2} to 10^{5} Hz with an amplitude of 20 mV at the open circuit potential (OCP). After the 120-day immersion, potentiodynamic polarization measurements were performed on CS Electrochemical Workstation. The potentiodynamic polarization curves were obtained by scanning from cathodic to the anodic direction (E_{OCP} ± 150 mV) at a scan rate of 0.2 mV s^{-1}. Besides, all measurements were implemented in a faraday cage to avoid external interference.

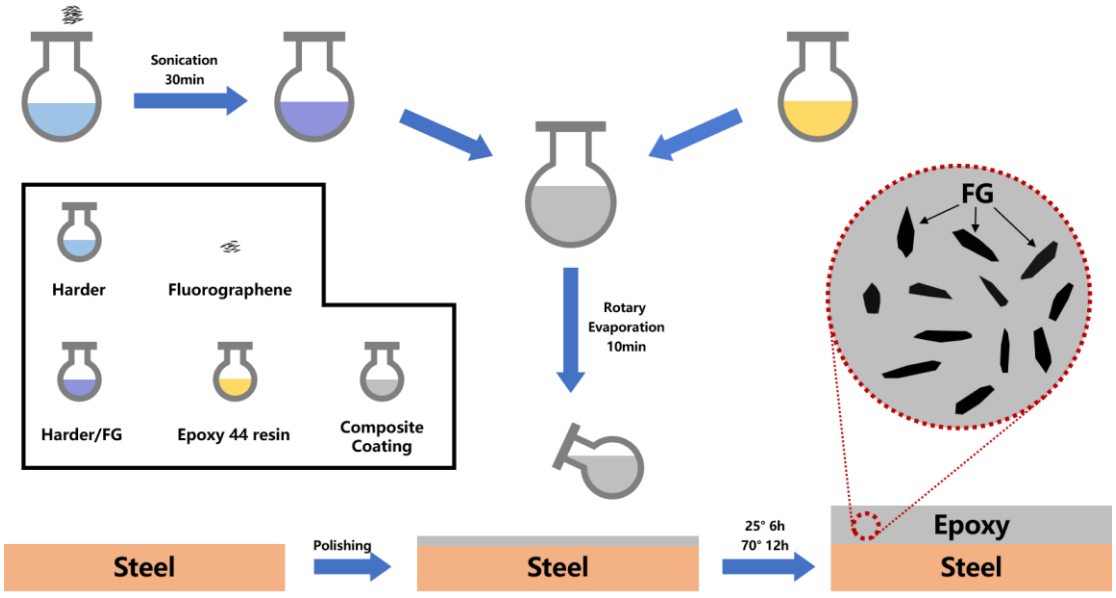

Figure 1. Schematic illustration of the preparation process of the FG/epoxy nanocomposite coatings.

3. RESULTS AND DISCUSSION

3.1. Characterization of GrF and FG.

The SEM image and EDS spectrum of the raw GrF powders are shown in Figure 2a, which indicate that GrF has a multilayered structure and the ratio of C and F is close to 1:1. The TEM image in Figure 2b shows the morphology of the prepared FG nanoplatelets, which is a few layered thin structure. The AFM image and the corresponding height profile of a single FG nanoplatelet are shown in Figure 2c and 2d, respectively. The quality of the exfoliated FG nanoplatelet is rather good and its thickness is about 3 nm. It has been reported that a single layered FG nanoplatelet has a thickness of 0.8 nm [40, 46]. Thus, the obtained FG nanoplatelets are estimated to have about 3~4 layers.

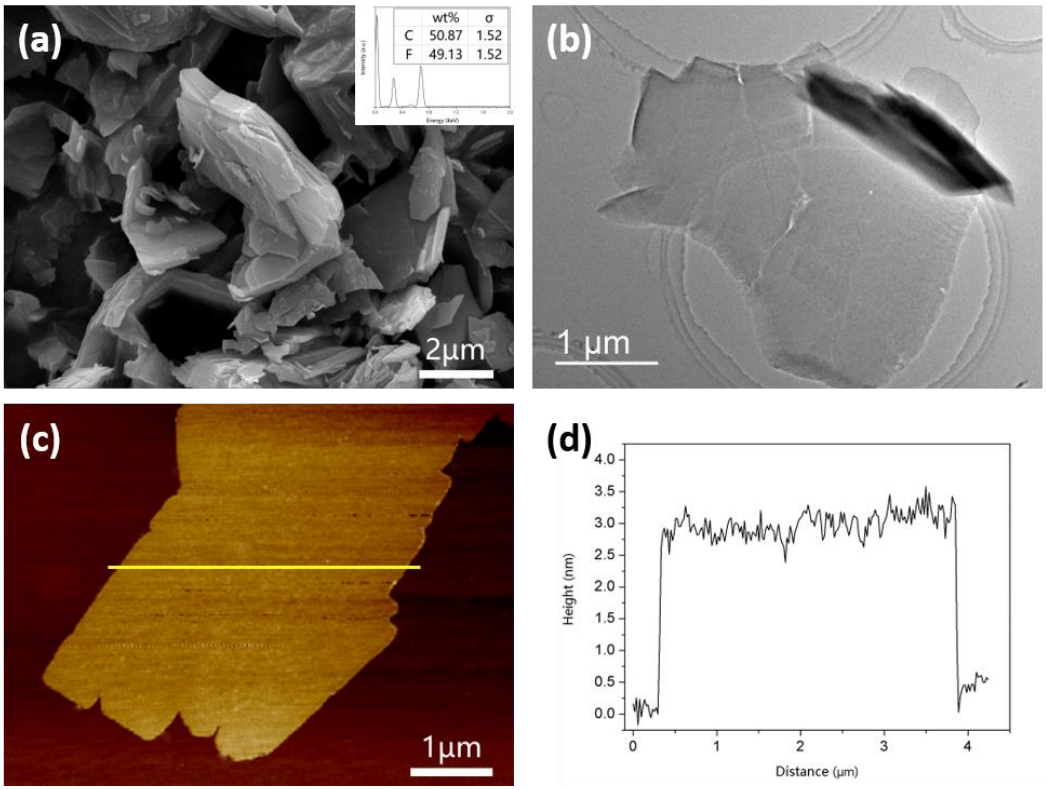

Figure 2. (a) SEM image of GrF, inset: EDS spectrum of GrF; (b) TEM image and (c) AFM image of FG; (d) height profile of the exfoliated FG nanoplatelet in AFM image.

3.2. Characterization of the FG/epoxy nanocomposite coatings.

To investigate the dispersion state of FG nanoplatelets in the epoxy matrixes, the cross-section morphologies of the FG/epoxy nanocomposite coatings were observed. The SEM images of the cross sections of different coating samples are shown in Figure 3. As shown in Figure 3a, the cross-section morphology of FG-0 wt% is very smooth without obvious micropores and microcracks which have been proved to be detrimental to the anticorrosion performance of coatings [19]. While for the nanocomposite coatings, the cross-section morphologies are quite rough and few micropores appear because of the

embedded FG nanoplatelets. As illustrated in Figure 3b, FG nanoplatelets have good dispersion in the epoxy matrix for FG-0.5 wt%. While for FG-1 wt%, a small amount of FG nanoplatelets tend to aggregate as shown in Figure 3c. With further increasing FG concentrations, obvious FG nanoplatelet agglomerations are found in the epoxy matrixes for FG-2 wt% and FG-3 wt%. The X-ray diffraction patterns of FG, FG-0 wt% and the FG/epoxy nanocomposite coatings are shown in Figure 3f. For the prepared FG nanoplatelets, the characteristic peak at about $2\theta = 13.8°$ is assigned to the (001) reflection from a hexagonal system for FG with high fluorine content [42, 47]. Besides, FG-0 wt% and the FG/epoxy nanocomposite coatings display a broad diffraction peak at around $2\theta = 17.5°$, demonstrating the amorphous nature of the epoxy matrixes [48, 49]. Obviously, the typical characteristic peak ($2\theta = 13.8°$) of FG is absent in the FG/epoxy nanocomposite coatings, which indicates the good compatibility between FG nanoplatelets and the epoxy matrixes.

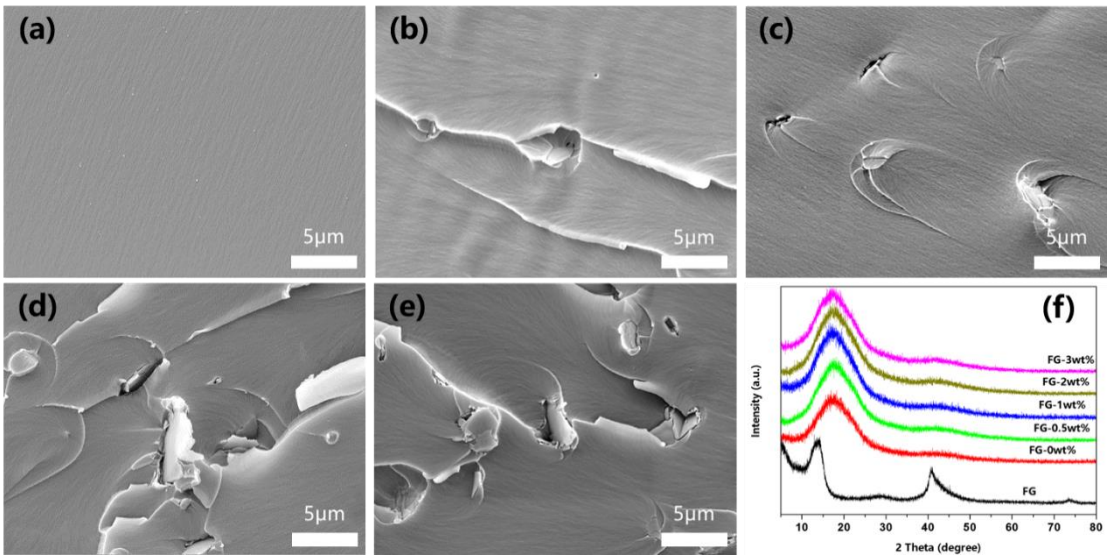

Figure 3. Cross-section morphologies of the coating samples: (a) FG-0 wt%, (b) FG-0.5 wt%, (c) FG-1 wt%, (d) FG-2 wt%, (e) FG-3 wt%; and (f) XRD patterns of FG and the coating samples.

3.3. Corrosion protection properties of the FG/epoxy nanocomposite coatings.

Electrochemical impedance spectroscopy is carried out to investigate the corrosion protection properties of the nanocomposite coatings containing various content of FG by measuring their dielectric properties. Figure 4 demonstrates the Bode plots of the prepared coatings for different immersion time. Generally, the impedance modulus at $f = 0.01Hz$ in the Bode-impedance plots are used to evaluate the barrier properties of coatings [50]. At the onset of the immersion test, all the coatings show high values of the $Z_{f=0.01Hz}$, which are close to $1.0 \times 10^{10}\ \Omega\ cm^2$ and attributed to the dense epoxy matrixes. With the immersion time prolonging, the $Z_{f=0.01Hz}$ value for FG-0 wt% gradually decreases. And the $Z_{f=0.01Hz}$ for FG-0 wt% is $1.14 \times 10^8\ \Omega\ cm^2$ after the 120-day immersion test in 3.5 wt% NaCl aqueous solution. By contrast, the $Z_{f=0.01Hz}$ for the nanocomposite coatings still show high values after the same immersion time, which are $3.15 \times 10^9\ \Omega\ cm^2$, $2.34 \times 10^9\ \Omega\ cm^2$, $2.67 \times 10^9\ \Omega\ cm^2$, $1.48 \times$

$10^9\ \Omega\ cm^2$ for FG-0.5 wt%, FG-1 wt%, FG-2 wt% and FG-3 wt%, respectively. Hence, it can be concluded that the anticorrosion performance of the pure epoxy coating has a more significant deterioration than that of the nanocomposite coatings containing FG nanoplatelets. Besides, it is observed that FG-0.5 wt% exhibits the highest value of the $Z_{f=0.01Hz}$ among all the coatings after the 120-day immersion test and the $Z_{f=0.01Hz}$ for FG-0.5wt% shows the minimum change during the whole immersion test, implying that the nanocomposite coating containing 0.5 wt% FG has the best corrosion protection property for the steel substrate. The high phase angle at a broad frequency range in the Bode-phase plots indicates that the coating can work as an isolating layer between the steel substrate and the external corrosive environment [51]. According to the Bode-phase plots in Figure 4b, the phase angle for FG-0 wt% at frequency range decreases significantly with the increase of the immersion time, suggesting the decrease of the corrosion protection property. For the nanocomposite coatings, the phase angles at entire frequency range also exist a decrease after the long-term immersion tests owing to the penetration of corrosive mediums. However, as compared with FG-0 wt%, the phase angles for the nanocomposite coatings show higher values, revealing that the nanocomposite coatings have better anticorrosion performance. At the high frequency region, the time constant corresponds to the response of coating matrixes, while at the low-medium frequency region, the time constant indicates the corrosion reactions at the interface between coating and steel substrate [37, 51, 52]. The Bode-phase plots for all the nanocomposite coatings in Figure 4 show that the coatings at the high frequency region have one time constant, whereas no time constant is found at the low-medium frequency region, which suggests that all the nanocomposite coatings still maintain excellent anticorrosion performance even after the 120-day immersion test. While for FG-0 wt%, at the low-medium frequency region a time constant is found after the 120-day immersion, suggesting that the coating had failed and the substrate was corroded because the corrosive mediums had permeated the epoxy matrix completely.

In order to quantitatively investigate the anticorrosion performance of FG-0 wt% and the nanocomposite coatings, the EIS results are then fitted by the Zview software. As shown in Figure 5a, the equivalent electric circuits are composed of the solution resistance R_s, the coating capacitance Q_c, the coating resistance R_c, the metal corrosion reaction resistance R_{ct} and the double-layer capacitance Q_{dl} [53-55]. The equivalent electric circuit (left in Figure 5a) is applied to fit the Bode plots of FG-0 wt% at the initial stage of the immersion test and the nanocomposite coatings for the whole immersion test, revealing that the coatings could prevent the penetration of corrosive mediums and provide corrosion protection for the steel substrates. After the 120-day immersion, the corrosive mediums reach the coating/substrate interface for FG-0 wt% and cause the corrosion reaction. The equivalent electric circuit (right in Figure 5a) is employed to fit the Bode plot of FG-0 wt% at the 120-day immersion. Figure 5b shows the fitting results of the coating resistance of all coatings. As demonstrated, the R_c of FG-0 wt% decreases from $1.49 \times 10^{10}\ \Omega\ cm^2$ to $9.86 \times 10^7\ \Omega\ cm^2$ after the 120-day immersion. On the contrary, the R_c of the nanocomposite coatings still maintain high values, which are at least an order of magnitude greater than that of FG-0 wt%. It is worth noting that FG-0.5 wt% has the highest value of R_c, which is $3.26 \times 10^9\ \Omega\ cm^2$ after the 120-day immersion. Consequently, the nanocomposite coatings show better corrosion protection properties during the long-term immersion tests than the pure epoxy coating, and the one containing 0.5 wt% FG exhibits the best anticorrosion performance.

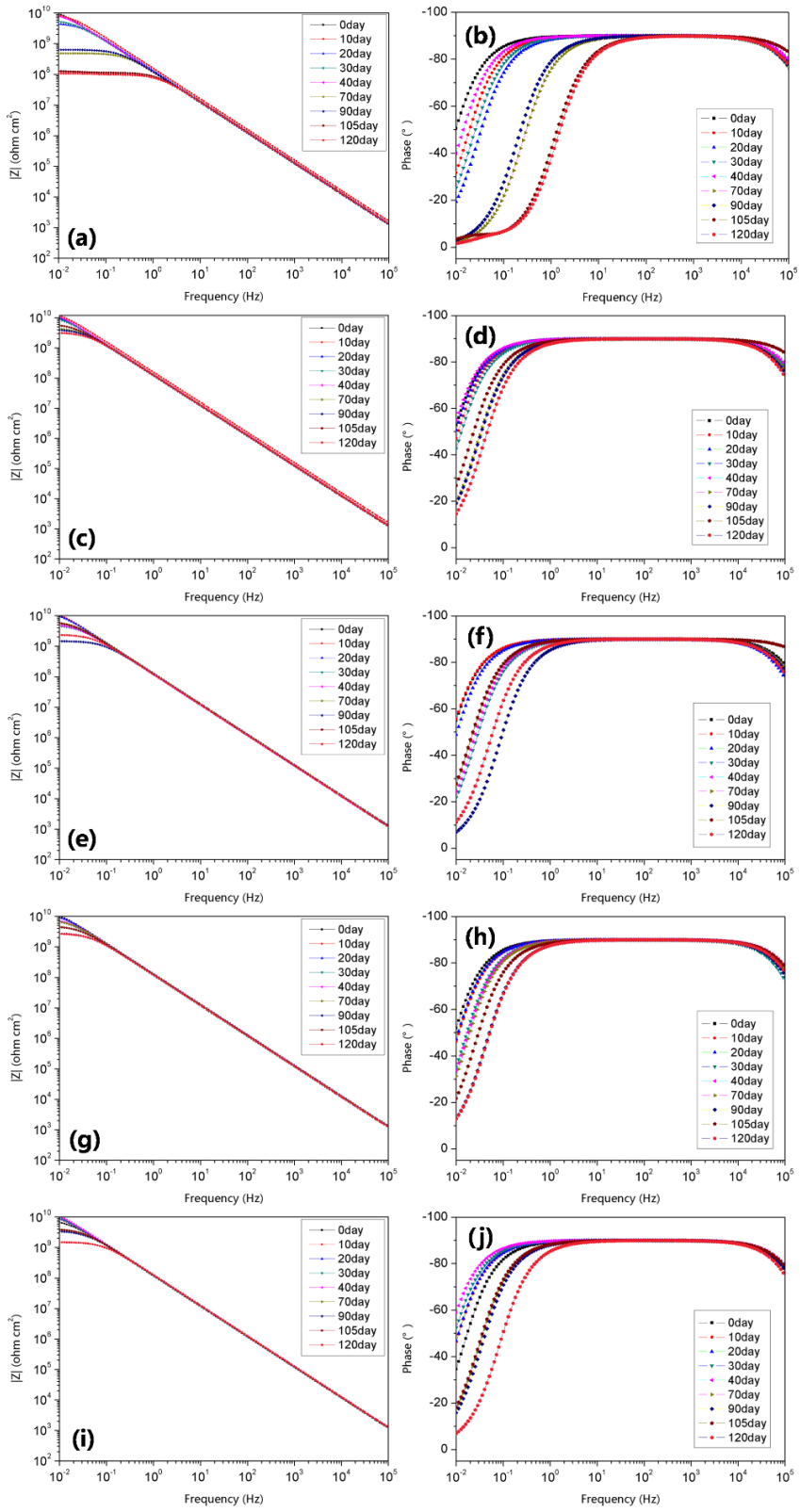

Figure 4. Bode plots of the coatings after the 120-day immersion tests in 3.5 wt% NaCl aqueous solution. (a)(b) FG-0 wt%, (c)(d) FG-0.5 wt%, (e)(f) FG-1 wt%, (g)(h) FG-2 wt%, (i)(j) FG-3 wt%.

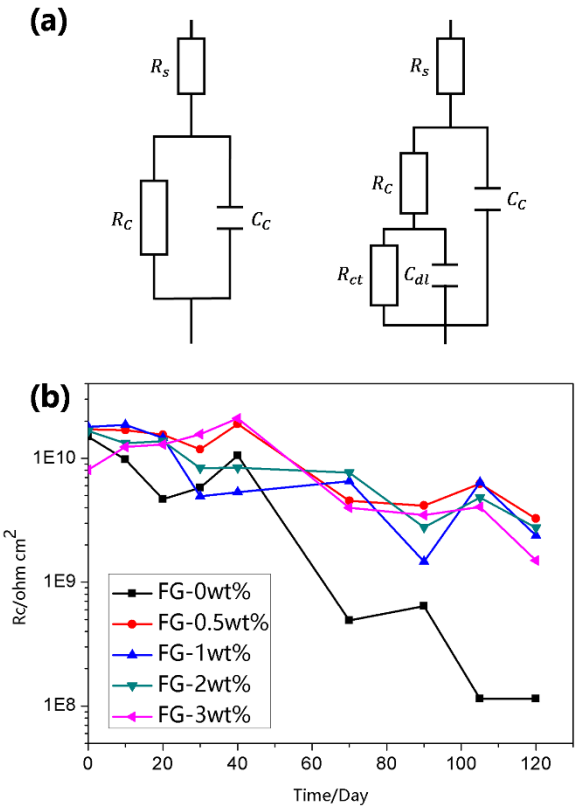

Figure 5. (a) Equivalent circuits and (b) the fitting results of the EIS results of different coatings.

The potentiodynamic polarization curves of the bare steel and the coated steel substrates in 3.5 wt% NaCl aqueous solution are presented in Figure 6. Some electrochemical parameters could be obtained by extrapolating Tafel plots, including the corrosion potential (E_{corr}) and the corrosion current density (I_{corr}) [56, 57]. Besides, the corrosion rate is also used to investigate the anticorrosion performance of the coatings. The corrosion rate (R_{corr}) is calculated from the following equation [37],

$$R_{corr} = \frac{kM_m I_{corr}}{n\rho_m}$$

where *k* is a constant with the value of 3268.5mol/A, M_m is the molar mass of metal substrate, n is the number of charge-transfer during corrosion reaction, ρ_m represents the density of metal substrate. All the electrochemical parameters are summarized in Table 1.

The polarization curves of the coated steel substrates are shown in Figure 6. The E_{corr} of the steel substrates protected by FG-0 wt%, FG-0.5 wt%, FG-1 wt%, FG-2 wt% and FG-3wt% are -0.421V, -0.338V, -0.342V, -0.353V and -0.414V, respectively. Regarding to the bare steel, the E_{corr} is -0.760V, which is more negative than that for the coated steel substrates, suggesting that FG-0 wt% and the nanocomposite coatings could effectively protect the steel substrates against corrosion. The E_{corr} for the steel substrate coated by FG-0.5 wt% has the most positive value among all the coating, which indicates the best corrosion protection property. Besides, the I_{corr} for FG-0 wt% and the nanocomposite coated substrates are close given by the polarization curves, which are lower than that for the bare steel (1.46×10^{-6} A/cm^2). Among all the coatings, the FG-0.5 wt% coated substrate exhibits the lowest I_{corr}, implying the best anticorrosion performance. Moreover, the results of the corrosion rate verify that FG-

0.5 wt% could provide the most effective protection for the steel substrate due to the lowest value of the corrosion rate.

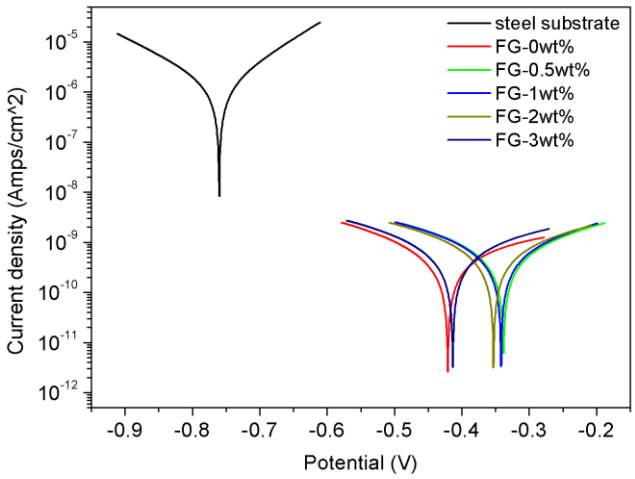

Figure 6. The polarization curves of the polished and coated steel substrates after the 120-day immersion in 3.5 wt% NaCl aqueous solution.

Table 1. The electrochemical parameters of the polished and coated steel substrates after the 120-day immersion in 3.5 wt% NaCl aqueous solution.

Sample	E_{corr} (V vs. AgCl)	I_{corr} (A/cm^2)	R_{corr} (mm/year)
Steel substrate	-0.760	1.46×10^{-6}	1.71×10^{-2}
FG-0 wt%	-0.421	1.62×10^{-9}	1.90×10^{-5}
FG-0.5 wt%	-0.338	1.11×10^{-9}	1.31×10^{-5}
FG-1 wt%	-0.342	1.14×10^{-9}	1.34×10^{-5}
FG-2 wt%	-0.353	1.41×10^{-9}	1.66×10^{-5}
FG-3 wt%	-0.414	1.56×10^{-9}	1.84×10^{-5}

Figure 7a shows the micrograph of the steel substrate after polishing and Figure 7(b-f) show the morphologies of the coated steel substrates after the 120-day immersion in 3.5 wt% NaCl aqueous solution. For the FG-0 wt% coating, obvious corrosion zones appear on the surface of the substrate, indicating that the substrate was corroded severely after the long-term immersion test. On the contrary, the substrates coated with the FG/epoxy nanocomposites have the similar morphologies with the pristine polished steel substrate, implying that the introduction of FG nanoplatelets in the epoxy matrixes could improve the long-term corrosion protection for the steel substrates. Clearly, the nanocomposite coatings have better corrosion protection properties in comparison to the pure epoxy coating, which agrees with the EIS results.

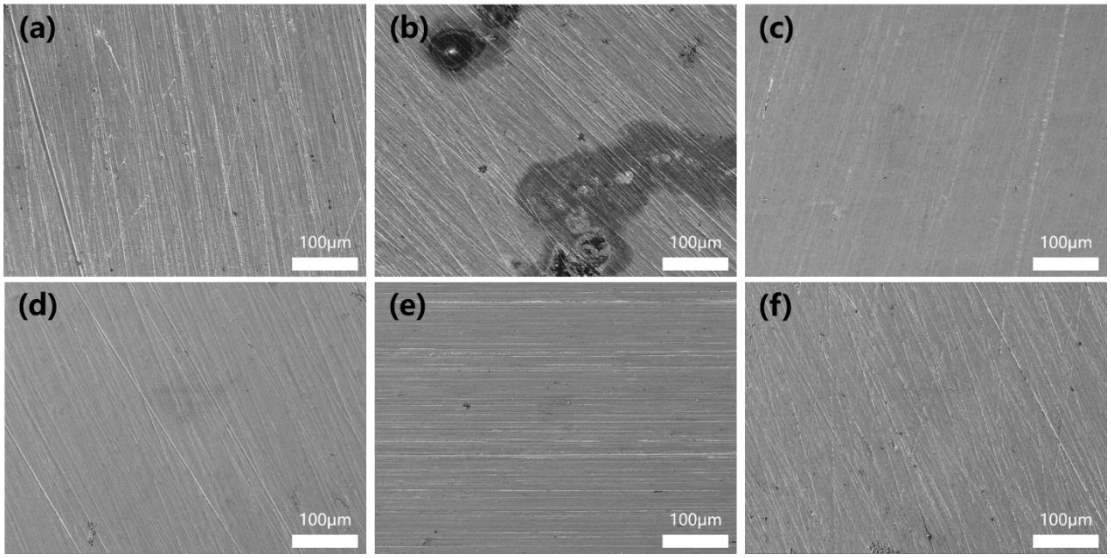

Figure 7. Micrographs of (a) the polished steel substrate and the coated steel substrates after the 120-day immersion in 3.5 wt% NaCl aqueous solution: (b) FG-0 wt%, (c) FG-0.5 wt%, (d) FG-1 wt%, (e) FG-2 wt%, and (f) FG-3 wt%.

3.4. Mechanism of anticorrosion of the FG/epoxy nanocomposite coatings

As a graphene derivative, fluorographene could effectively enhance the corrosion protection properties of the epoxy matrixes due to its molecule impermeability inherited from graphene. The FG nanoplatelets, dispersed in the epoxy matrixes, can enhance the diffusion resistance of the chloride ion, oxygen and water molecules by prolonging the diffusion pathway of them, thus decreasing the corrosion rate and prolonging the life of the coatings, as schematically shown in Figure 8. Besides, the hydrophobicity of the coatings increases owing to the incorporation of FG (Figure S1), which could also inhibit the diffusion of corrosive mediums effectively [58], contributing to the improvement of the anticorrosion performance of the nanocomposite coatings. As for the nanocomposite coatings containing different FG contents, FG-0.5 wt% shows the best anticorrosion performance because a small amount of FG nanoplatelets could be dispersed in the epoxy matrix uniformly without any agglomeration. While for the other nanocomposite coatings, lots of agglomerations are formed due to the addition of a large amounts of FG nanoplatelets, which lead to the heterogeneous barrier properties of the coatings.

For comparison, the graphene/epoxy nanocomposite coating with 0.5 wt% content of graphene (G) was manufactured, marked as G-0.5 wt%. As shown Figure S3, G-0.5 wt% with a low impedance modulus had failed after 70 days of immersion due to a large amount of micropores formed in the epoxy matrix caused by the bad dispersion of graphene sheets (Figure S2). Hence, the anticorrosion performance of the pure epoxy coating and the FG/epoxy nanocomposite coatings are better than that of G-0.5 wt%. Moreover, FG show the electrical insulation properties due to the introduction of fluorine, which can inhibit the anodic and cathodic processes of the corrosion reactions [40, 59]. Therefore, as compared with graphene, FG is supposed to exhibit better corrosion protection behavior.

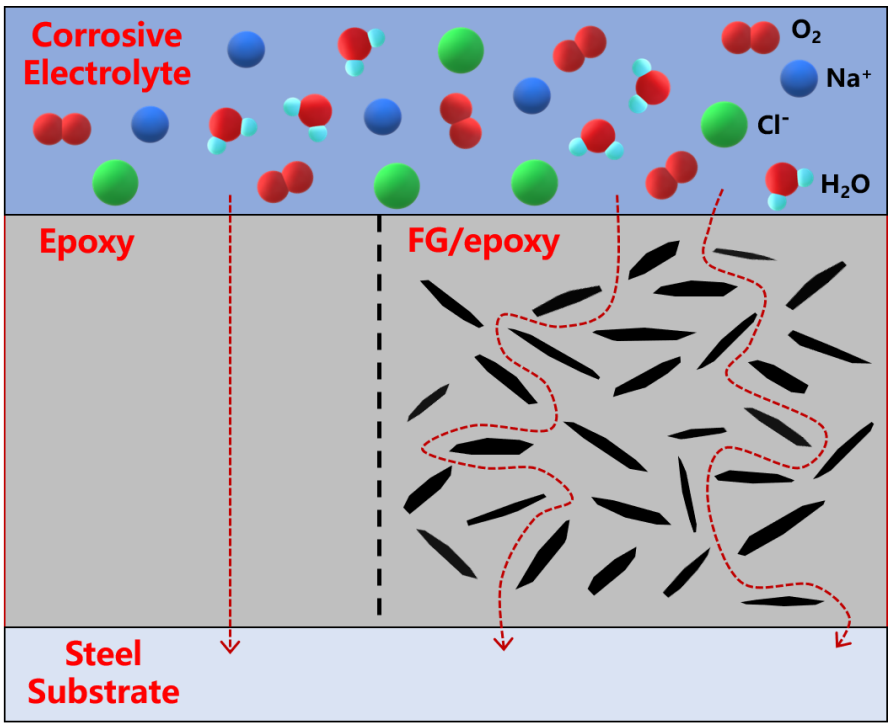

Figure 8. Schematic diagram of the corrosion protection mechanism of the FG/epoxy nanocomposite coatings through prolonging the diffusion pathway of H_2O, O_2, Na^+ and Cl^-.

4. CONCLUSION

Fluorographene (FG), prepared from graphite fluoride (GrF) through a microwave-assisted liquid phase exfoliation method, has been used as nano-filler in the epoxy matrix to prepare corrosion protection coatings for the steel substrates through an environment friendly solventless method. The EIS and the potentiodynamic polarization measurement indicate that the nanocomposite coatings show highly enhanced corrosion protection properties against corrosive environment for the long-term immersion tests when compared to the pure epoxy coating. Moreover, the nanocomposite coating containing 0.5 wt% content of FG has the best anticorrosion performance because a small amount of FG nanoplatelets have good dispersion in the epoxy matrix. The FG molecule impermeability and the improved hydrophobicity of the composite coating are beneficial for the improvement of the anticorrosion performance of the nanocomposite coatings through the extension of the diffusion pathway of corrosive mediums. Besides, the electrical insulation of FG nanoplatelets in the matrix is thought as another important factor that enables the nanocomposite coatings to isolate the anodic and cathodic regions of the corrosion reaction on the steel substrates. The enhanced anticorrosion performance of the nanocomposite coatings in our current study demonstrates that fluorographene, as a substitute for graphene, can be used as a novel anticorrosion nano-filler for applications in the corrosion protection industry.

SUPPORTING INFORMATION

The contact angles of the prepared nanocomposite coatings are exhibited in Figure S1. Clearly, the pure epoxy coating, named FG-0 wt%, shows a hydrophilic nature with the contact angle of 70°. With the incorporation of FG nanoplatelets, the contact angles of the nanocomposite coatings increase. In detail, the contact angle increases to 87° for FG-0.5wt% and that of FG-1wt%, FG-2wt% and FG-3wt% are greater than 90°, indicating that those nanocomposite coatings are hydrophobic.

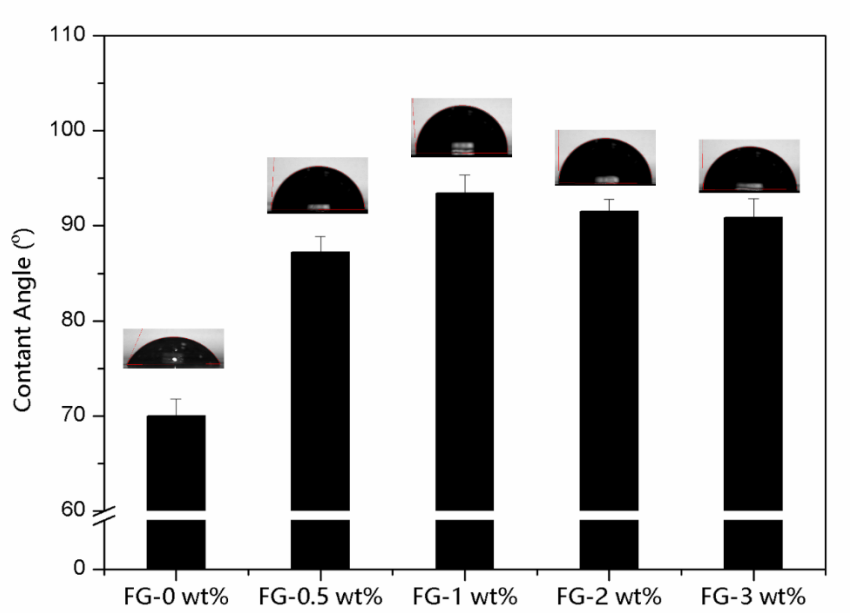

Figure S1. Contact angles of FG-0 wt% and the nanocomposite coatings.

According to the above studies, the FG-0.5wt% coating has the best anticorrosion performance for the long-term immersion test. Therefore, the same preparation process was carried out to prepare graphene/epoxy nanocomposite coating with 0.5 % content of graphene (G) and the prepared G/epoxy nanocomposite coating was marked as G-0.5wt%. The raw G sheets was purchased from The Sixth Element (Changzhou) materials technology Co, Ltd. The cross-section of the G/epoxy nanocomposite coating was observed by SEM and the electrochemical property of the G/epoxy nanocomposite coating was studied.

Figure S2 shows the SEM images of the cross section of G-0.5wt%. Apparently, the cross-section morphology of G-0.5wt% is rough and numerous micropores are formed because of the aggregation of graphene sheets in the matrix. Figure S3 presents the Bode plots of G-0.5wt% under different immersion time. At the beginning of the immersion test, the G/epoxy nanocomposite coating has an impedance modulus of $1.8 \times 10^8\ \Omega\, cm^2$ at $f = 0.01Hz$, which is two orders of magnitude smaller than that of FG-0 wt% and the FG/epoxy nanocomposite coatings. With the immersion time increasing, the $Z_{f=0.01Hz}$ of G-0.5wt% decreases significantly due to the micropores in the matrix caused by the bad dispersion of graphene sheets. After 70 days of immersion, the phase angle of G-0.5 wt% decreases significantly and

at the low-medium frequency region a time constant is found, suggesting that the prepared G-0.5 wt% coating was failed.

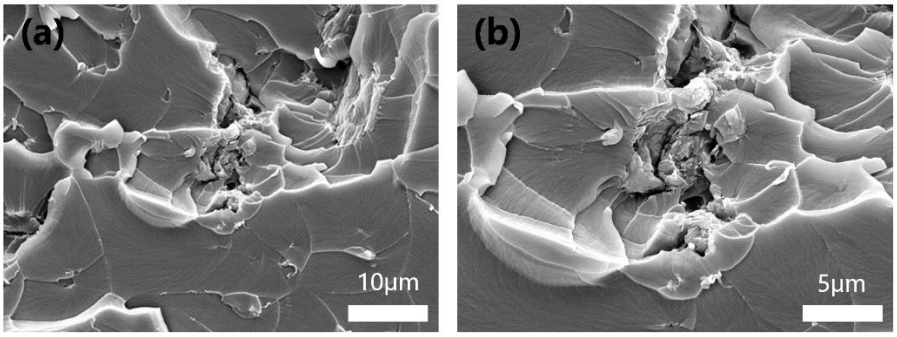

Figure S2. Cross-sectional morphologies of G-0.5wt%: (a) 5kx magnification and (b) 10kx magnification.

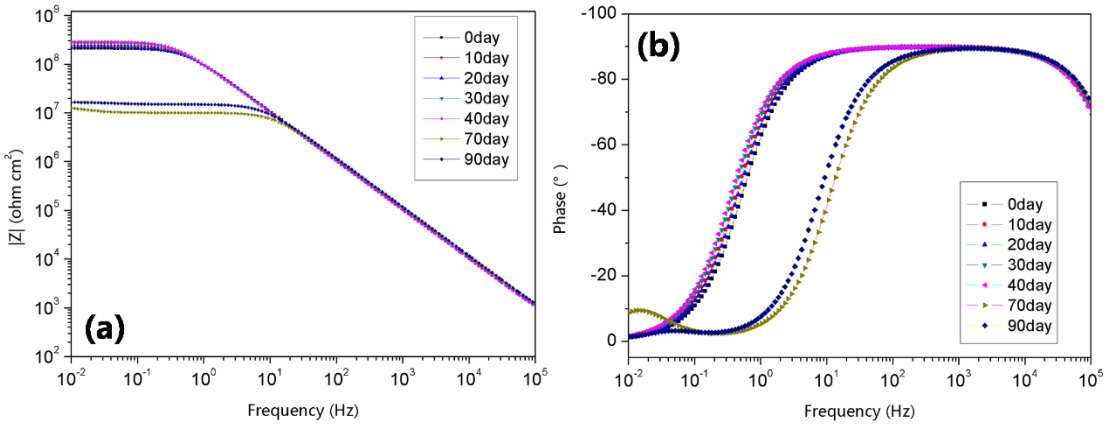

Figure S3. Bode plots of G-0.5wt% after the 70-day immersion in 3.5 wt% NaCl aqueous solution.

ACKNOWLEDGEMENT

This work was supported by the start-up funding from Southern University of Science and Technology (SUSTech), "The Recruitment Program of Global Youth Experts of China", the Foundation of Shenzhen Science and Technology Innovation Committee (Grant No.: JCYJ20170817110440310, KQJSCX20170726145415637), and China Postdoctoral Science Foundation (Grant No.: 2018M641634).

Reference

1. M. Behzadnasab, S.M. Mirabedini, K. Kabiri, S. Jamali, *Corrosion Sci.*, 53 (2011) 89-98.
2. J.D. Brassard, D.K. Sarkar, J. Perron, A. Audibert-Hayet, D. Melot, *J. Colloid Interface Sci.*, 447 (2015) 240-247.
3. Y.N. Kok, P.E. Hovsepian, Q. Luo, D.B. Lewis, J.G. Wen, I. Petrov, *Thin Solid Films*, 475 (2005) 219-226.
4. C.H. Chang, T.C. Huang, C.W. Peng, T.C. Yeh, H.I. Lu, W.I. Hung, C.J. Weng, T.I. Yang, J.M. Yeh, *Carbon*, 50 (2012) 5044-5051.
5. J. Khodabakhshi, H. Mandavi, F. Najafi, *Corrosion Sci.*, 147 (2019) 128-140.

6. S. John, A. Salam, A.M. Baby, A. Joseph, *Prog. Org. Coat.*, 129 (2019) 254-259.
7. D. Thierry, D. Persson, G. Luckeneder, K.H. Stellnberger, *Corrosion Sci.*, 148 (2019) 338-354.
8. Q. Liu, R.N. Ma, A. Du, X.R. Zhang, Y.Z. Fan, X. Zhao, S.H. Zhang, X.M. Cao, *Corrosion Sci.*, 150 (2019) 64-75.
9. S. Pourhashem, M.R. Vaezi, A. Rashidi, M.R. Bagherzadeh, *Prog. Org. Coat.*, 111 (2017) 47-56.
10. H. Lu, S.T. Zhang, W.H. Li, Y.A. Cui, T. Yang, *ACS Appl. Mater. Interfaces*, 9 (2017) 4034-4043.
11. B. Ramezanzadeh, S. Niroumandrad, A. Ahmadi, M. Mahdavian, M.H.M. Moghadam, *Corrosion Sci.*, 103 (2016) 283-304.
12. B. Ramezanzadeh, E. Ghasemi, M. Mahdavian, E. Changizi, M.H.M. Moghadam, *Carbon*, 93 (2015) 555-573.
13. M.D. Maksimovic, V.B. Miskovicstankovic, *Corrosion Sci.*, 33 (1992) 271-279.
14. H. Vakili, B. Ramezanzadeh, R. Amini, *Corrosion Sci.*, 94 (2015) 466-475.
15. J.H. Ding, O.U. Rahman, W.J. Peng, H.M. Dou, H.B. Yu, *Appl. Surf. Sci.*, 427 (2018) 981-991.
16. A. Bahrani, R. Naderi, M. Mahdavian, *Prog. Org. Coat.*, 120 (2018) 110-122.
17. X.H. Liu, C.J. Gu, Z.H. Wen, B.R. Hou, *Prog. Org. Coat.*, 115 (2018) 195-204.
18. Z. Mirzakhanzadeh, A. Kosari, M.H. Moayed, R. Naderi, P. Taheri, J.M.C. Mol, *Corrosion Sci.*, 138 (2018) 372-379.
19. Y.W. Ye, D.W. Zhang, T. Liu, Z.Y. Liu, W. Liu, J.B. Pu, H. Chen, H.C. Zhao, X.G. Li, *J. Hazard. Mater.*, 364 (2019) 244-255.
20. M. Mahdavian, M.M. Attar, *Prog. Org. Coat.*, 53 (2005) 191-194.
21. Y.S. Hao, F.C. Liu, E.H. Han, S. Anjum, G.B. Xu, *Corrosion Sci.*, 69 (2013) 77-86.
22. B. Ramezanzadeh, M. Khazaei, A. Rajabi, G. Heidari, D. Khazaei, *Corrosion*, 70 (2014) 56-65.
23. Y.S. Hao, F.C. Liu, E.H. Han, *J. Electrochem. Soc.*, 159 (2012) C403-C410.
24. A. Ghanbari, M.M. Attar, *J. Ind. Eng. Chem.*, 23 (2015) 145-153.
25. M.G. Hosseini, P.Y. Sefidi, *Surf. Coat. Technol.*, 331 (2017) 66-76.
26. M. Rostami, S. Rasouli, B. Ramezanzadeh, A. Askari, *Corrosion Sci.*, 88 (2014) 387-399.
27. M.G. Sari, B. Ramezanzadeh, M. Shahbazi, A.S. Pakdel, *Corrosion Sci.*, 92 (2015) 162-172.
28. F.W. Jiang, W.J. Zhao, Y.M. Wu, J.D. Dong, K.H. Zhou, G.M. Lu, J.B. Pu, *Prog. Org. Coat.*, 127 (2019) 70-79.
29. S. Pourhashem, M.R. Vaezi, A. Rashidi, M.R. Bagherzadeh, *Corrosion Sci.*, 115 (2017) 78-92.
30. Y.W. Ye, D.W. Zhang, T. Liu, Z.Y. Liu, J.B. Pu, W. Liu, H.C. Zhao, X.G. Li, L.P. Wang, *Carbon*, 142 (2019) 164-176.
31. L. Liu, S.M. Ryu, M.R. Tomasik, E. Stolyarova, N. Jung, M.S. Hybertsen, M.L. Steigerwald, L.E. Brus, G.W. Flynn, *Nano Lett.*, 8 (2008) 1965-1970.
32. R.R. Nair, P. Blake, A.N. Grigorenko, K.S. Novoselov, T.J. Booth, T. Stauber, N.M.R. Peres, A.K. Geim, *Science*, 320 (2008) 1308-1308.
33. Z.S. Wu, W.C. Ren, L.B. Gao, J.P. Zhao, Z.P. Chen, B.L. Liu, D.M. Tang, B. Yu, C.B. Jiang, H.M. Cheng, *ACS Nano*, 3 (2009) 411-417.
34. V. Berry, *Carbon*, 62 (2013) 1-10.
35. J.S. Bunch, S.S. Verbridge, J.S. Alden, A.M. van der Zande, J.M. Parpia, H.G. Craighead, P.L. McEuen, *Nano Lett.*, 8 (2008) 2458-2462.
36. C.L. Cui, A.T.O. Lim, J.X. Huang, *Nat. Nanotechnol.*, 12 (2017) 834-835.
37. W. Sun, L.D. Wang, T.T. Wu, Y.Q. Pan, G.C. Liu, *Carbon*, 79 (2014) 605-614.
38. Y.H. Yu, Y.Y. Lin, C.H. Lin, C.C. Chan, Y.C. Huang, *Polym. Chem.*, 5 (2014) 535-550.
39. L. Gu, S. Liu, H.C. Zhao, H.B. Yu, *ACS Appl. Mater. Interfaces*, 7 (2015) 17641-17648.
40. M. Zhang, Y.C. Ma, Y.Y. Zhu, J.F. Che, Y.H. Xiao, *Carbon*, 63 (2013) 149-156.
41. R.R. Nair, W. Ren, R. Jalil, I. Riaz, V.G. Kravets, L. Britnell, P. Blake, F. Schedin, A.S. Mayorov, S. Yuan, M.I. Katsnelson, H.M. Cheng, W. Strupinski, L.G. Bulusheva, A.V. Okotrub, I.V. Grigorieva, A.N. Grigorenko, K.S. Novoselov, A.K. Geim, *Small*, 6 (2010) 2877-2884.
42. P.W. Gong, Z.F. Wang, J.Q. Wang, H.G. Wang, Z.P. Li, Z.J. Fan, Y. Xu, X.X. Han, S.R. Yang, *J.*

Mater. Chem., 22 (2012) 16950-16956.
43. F. Lei, C.T. Zhang, Z.P. Cai, J.L. Yang, H.Y. Sun, D.Z. Sun, *Polymer*, 150 (2018) 44-51.
44. F. Lei, M. Yang, F. Jiang, H. Zhang, Z. Zhang, D.Z. Sun, *Chem. Eng. J.*, 360 (2019) 673-679.
45. S. Pourhashem, M.R. Vaezi, A. Rashidi, *Surf. Coat. Technol.*, 311 (2017) 282-294.
46. H.Q. Yao, S.A. Hawkins, H.J. Sue, *Compos. Sci. Technol.*, 146 (2017) 161-168.
47. P.P. Zhang, J.P. Zhao, K. Zhang, R. Bai, Y.M. Wang, C.X. Hua, Y.Y. Wu, X.X. Liu, H.B. Xu, Y. Li, *Compos. Pt. A-Appl. Sci. Manuf.*, 84 (2016) 428-434.
48. M.K. Shukla, K. Sharma, *Mater. Res. Express*, 6 (2019) 125323.
49. D. Liu, W.J. Zhao, S. Liu, Q.H. Cen, Q.J. Xue, *Surf. Coat. Technol.*, 286 (2016) 354-364.
50. C. Chen, S.H. Qiu, M.J. Cui, S.L. Qin, G.P. Yan, H.C. Zhao, L.P. Wang, Q.J. Xue, *Carbon*, 114 (2017) 356-366.
51. M. Mahdavian, M.M. Attar, *Corrosion Sci.*, 48 (2006) 4152-4157.
52. S. Liu, L. Gu, H.C. Zhao, J.M. Chen, H.B. Yu, *J. Mater. Sci. Technol.*, 32 (2016) 425-431.
53. X. Wei, H. Xue, J. Wang, W. Tao, S. Li, G. Hu, X. Fan, G. Hao, J. He, *Carbon*, 101 (2016) 315-323.
54. G.Y. Zhu, X.K. Cui, Y. Zhang, S.G. Chen, M.Y. Dong, H. Liu, Q. Shao, T. Ding, S.D. Wu, Z.H. Guo, *Polymer*, 172 (2019) 415-422.
55. M.J. Cui, S.M. Ren, H.C. Zhao, Q.J. Xue, L.P. Wang, *Chem. Eng. J.*, 335 (2018) 255-266.
56. L.L. Zhang, S.J. Liu, H.C. Han, Y. Zhou, S.C. Hu, C. He, Q.X. Yan, *Surf. Coat. Technol.*, 341 (2018) 95-102.
57. W.N. Shen, L.J. Feng, X. Liu, H. Luo, Z. Liu, P.R. Tong, W.H. Zhang, *Prog. Org. Coat.*, 90 (2016) 139-146.
58. D.W. Li, H.Y. Wang, Y. Liu, D.S. Wei, Z.X. Zhao, *Chem. Eng. J.*, 367 (2019) 169-179.
59. Z.Q. Yang, W. Sun, L.D. Wang, S.J. Li, T.Z. Zhu, G.C. Liu, *Corrosion Sci.*, 103 (2016) 312-318.

© 2020 The Authors. Published by ESG (www.electrochemsci.org). This article is an open access article distributed under the terms and conditions of the Creative Commons Attribution license (http://creativecommons.org/licenses/by/4.0/).